A Theoretical Analysis of Absorption Spectra of Photosynthetic Reaction Centers: Mechanism of Temperature Dependent Peak Shift

C. H. Chang,*,†,‡ M. Hayashi,|| K. K. Liang,‡ R. Chang,‡ and S. H. Lin†,‡,§

Department of Chemistry, National Taiwan University, Taipei 106, Taiwan R.O.C., Institute of Atomic and Molecular Sciences, Academia Sinica, P.O. Box 23-166, Taipei 106, Taiwan R.O.C., and Department of Chemistry and Biochemistry, Arizona State University, Tempe, Arizona 85287-1604

Received: June 7, 2000; In Final Form: October 25, 2000

Detailed analysis of the absorption spectra of the R26.Phe-a mutant RCs at various temperatures has been presented constructing a model Hamiltonian based on the previous spectral analysis results. The temperature dependence of the electronic asymmetry and the coupling between the Bchls in the special pair can be obtained by using the thermal expansion model. The major contributions to the energy gaps between the exciton states of the special pair result from the protein-induced electronic asymmetry Δ and the intra-dimer coupling β. The values of Δ and β are obtained to be 147 and 405.19 cm^{-1} at room temperature, respectively, and they increase with a decrease in temperature. Peak intensity ratios of each electronic state to the lowest electronic state at various temperatures are calculated using the delocalized basis set. The absorption spectra at 77 and 278 K have been theoretically predicted by using the model presented in this paper. Anisotropy is also studied using both delocalized and dimer basis set. The anisotropy values are found to depend on a choice of basis sets.

I. Introduction

The photosynthetic reaction center (RC) of the purple nonsulfur bacteria consists of several chromophores.[1−52] For example, *Rb. sphaeroides*, one of the best-characterized RC, contains six chromophores.[29] Two bacteriochlorophyll *a* (Bchl-a) molecules together form an electronically coupled pair, known as special pair P, situated near the peri-plasma side of the membrane. The other two monomer Bchl-a (accessory Bchl, or B) and two bacteriopheophytin *a* (Bphe-a, or H) molecules are arranged below P in sequence. These six chromophores are embedded in the protein environment to constitute a pigment−protein complex with an approximately 2-fold symmetry forming two branches L and M. The L branch, for example, consists of P_L (Bchl in P at the L branch side), B_L, and H_L components. Because of the different protein surroundings, these two branches are not identical.

Many kinds of mutants have so far been prepared using genetic engineering techniques applied to mutate either the chromophores or protein residues for various investigations. The most commonly used mutant for spectroscopic and dynamic studies is the R26 mutant. This mutant can be generated by removing the carotenoids (Car) from the wild type (WT) RC of *Rb. sphaeroides*. Because of lacking of the interaction between Car and the chromophores, the R26 mutant can be a simple system for spectroscopic and dynamic investigations.

One of the most basic spectroscopic characteristics of RCs can be obtained from absorption spectra. For example, the absorption spectra of the RCs of both WT and R26 exhibit three broad bands in the near-IR region (10500 ∼ 14000 cm^{-1}).[39,42] In particular, the broad bands of R26 appear in 870, 800, and 760 nm at room temperature. These bands were conventionally assigned as the Q_y electronic transitions of P (870 nm), B (800 nm), and H (760 nm) components of RCs.

Recent studies have proposed a more detailed origin of these bands. Considering the fact that P is a dimer, the 870 nm band has been assigned to the P_- band, the lower exciton band of special pair. Quite recently, the location of the P_+ band, the higher exciton band of special pair, has been proposed to be around 810 nm at room temperature and thus this band is merged in the B band.[51,53] On the basis of analysis of the resonance Raman spectra of the R26 RCs, Mathies et al. proposed a two-electronic-state model for the two monomer Bchls (B).[42] In addition, their analysis also provided the vibronic properties of P, B, and H such as vibrational frequencies, their Huang−Rhys factors, and the electronic transition frequencies. These studies indicate that more than three electronic states are needed to understand the origin of the P, B, and H bands.

Theoretical and experimental investigations on the nature of the electronic states involved in the P bands have attracted much attention.[54−60] For example, Parson and co-workers investigated the couplings of P_- and P_+ with the internal charge transfer (CT) states from the microscopic theoretical point of view.[54] The involvement of the internal CT states to P_- and P_+ is still under debate (see ref 58 for more detailed review).

Another interesting feature in the absorption spectra of RCs is that the P band of R26 exhibits a very large peak shift with temperature. Moreover, recent anisotropy analysis suggested that the peak intensity of the P_- transition is 10 times larger than that of the P_+ transition at room temperature.[51,53] Meanwhile, such a temperature-dependent peak shift cannot be seen in the B and H bands. The absorption spectra of R26.Phe-a mutants (a chromophore-mutated mutant) at various temperatures show a very similar temperature dependence in P and B bands.[52] Note

* To whom correspondence should be addressed. E-mail:chchang@pub.iams.sinica.edu.tw.
† Department of Chemistry.
‡ Institute of Atomic and Molecular Sciences.
§ Department of Chemistry and Biochemistry.
|| Center for Condensed Matter Sciences, National Taiwan University.

10.1021/jp0020438 CCC: $20.00
Published on Web 01/23/2001

TABLE 1: The 0−0 Transitions of the P_-, P_+ and B Bands and the Peak Intensity Patios of B/P_- and P_+/P_-[a]

	0−0 transition			peak ratio	
	P_-	P_+	B $S = 0.8$ (34 cm^{-1})	B/P_-	P_+/P_-
R26.Phe-a 50K	10975.6	12275.6	12404 (806.2 nm) 12504 (799.7 nm)	1.34	0.267
R26.Phe-a 100 K	11010.6	12240.6	12404 12504	1.265	0.237
R26.Phe-a 150 K	11070.6	12215.6	12404 12504	1.180	0.210
R26.Phe-a 200 K	11130.6	12180.6	12404 12504	1.128	0.209
R26.Phe-a 250 K	11190.6	12150.6	12404 12504	1.010	0.130
R26.Phe-a 295 K	11265.6	12110.6	12404 12504	0.988	0.05
R26 77 K	10982.6	12250.6	12400 12475	1.27	0.368
R26 85 K	10975.6	12220.6	12440 12500	1.42	0.168
R26 298 K	11257.6	12150.6	12400 12475	0.974	0.082
WT 1 K	10920.6	12270.6	12440 12440	1.091	0.517
WT 12 K	10940.6	12275.6	12440 12440	0.958	0.517

[a] These data are obtained by the simulations of the absorption curves of the RCs of wild type, R26 and R26.Phe-a mutants of *Rb. sphaeroides* at different temperatures.

that R26.Phe-a mutants are mutated from R26 by replacing the two Bphe-a molecules with two plant pheophytins.

In previous studies,[61,62] we simulated the absorption spectra of the R26 and R26Phe-a mutants using a four electronic states model and obtained the transition moment intensity ratio of P_+ to P_- and that of B to P_-. In our model, we assumed that the lowest and second lowest optical transitions were associated with dimer state P_- and P_+, respectively. Two different transitions due to the two monomer Bchls were also included in the model. Applying this model to absorption spectral analysis, we investigated temperature dependence of the P and B bands of the mutant RCs of *Rb. sphaeroides* R26 and R26.Phe-a. We assigned the frequencies of the electronic transitions from the ground state to these four electronic states as listed in Table 1 and proposed the vibrational modes of each electronic state.[61,62] We also obtained the peak intensity ratios among these electronic transitions. In the previous analysis, we found that with an increase in temperature the optical transitions of the P_- and P_+ of R26 and R26.Phe-a exhibit blue and red shifts in the absorption spectra, respectively. Moreover, both the peak intensity ratios of the P_+ and two Bchls bands to the P_- band decrease with increased temperature. To consider the temperature-dependent peak shift of the P band of R26 RC, we have proposed a thermal expansion model.

The purpose of this study is to construct a model Hamiltonian based on the previous spectral analysis results.[62] We would like to map the temperature-dependent peak shift of the P band of R26 RC onto this model Hamiltonian using a delocalized state description. For comparison, a dimer model is also discussed. The rest of this paper is organized as follows. Section II presents a general theory for absorption spectra of multielectronic and multivibrational systems. To describe the electronic states involved in absorption spectra, a delocalized state description and a dimer model are introduced. Section III investigates the temperature-dependent peak shift of the P band of R26.Phe-a mutants and discusses the interactions between chromophores and the angles between the transition dipole moments of the Bchls at various temperatures. This section also summarizes the main results of this work.

II. Theory

A. Absorption Spectra for Multielectronic and Multivibronic Systems. Ordinary steady state absorption spectra involve the electronically ground vibronic manifold $\{gu\}$ and several electronically excited vibronic manifolds $\{e_k\upsilon_k\}_{k=1...N}$ with N being the number of electronic states.[63,64] In this case, the absorption coefficient is given by

$$\alpha(\omega) = \sum_{k=1}^{N} \alpha_{e_k g}(\omega) \tag{1a}$$

where

$$\alpha_{e_k g}(\omega) = \frac{4\pi^2\omega}{3\hbar c n_{e_k}(\omega)} \sum_{\upsilon_k} \sum_{u} P_{\mathrm{gu}} |\langle \Psi_{e_k\upsilon_k} | \vec{\mu} | \Psi_{\mathrm{gu}} \rangle|^2 D(\omega_{e_k\upsilon_k,\mathrm{gu}} - \omega) \tag{1b}$$

In eq 1b, P_{gu} represents the Boltzmann factor, ω is the optical frequency, $D(\omega_{e_k\upsilon_k,\mathrm{gu}} - \omega)$ is the line-shape function, and $\Psi_{e_k\upsilon_k}$ and Ψ_{gu} represent the molecular wave functions. In the case of displaced harmonic potential surfaces with inhomogeneity in the electronic energy gap, eq 1 reduces to

$$\langle \alpha_{e_k g}(\omega) \rangle = \frac{2\pi\omega}{3\hbar c n_{e_k}(\omega)} |\vec{\mu}_{e_k g}|^2 \times \mathrm{Re} \int_0^\infty \mathrm{d}t \exp[it(\omega - \bar{\omega}_{e_k g}) - t\gamma_{e_k g} - (tD_{e_k g}/2)^2] G_{e_k g}(t) \tag{2a}$$

where

$$G_{e_k g}(t) = \exp[-\sum_{j=1}^{N_k} S_{kj}\{(2\bar{n}_{kj} + 1) - (\bar{n}_{kj} + 1)\mathrm{e}^{it\omega_{kj}} - \bar{n}_{kj}\mathrm{e}^{-it\omega_{kj}}\}] \tag{2b}$$

The Condon approximation has been applied to eq 2a. Here $\vec{\mu}_{e_k g}$ represents the electronic transition dipole moments between the electronic state e_k and the electronic ground state g, $\hbar\omega_{kj}$ stands for the vibrational energy of the jth mode of the kth electronic state, S_{kj} is its coupling constant (Huang−Rhys factor), $D_{e_k g}$ is the inhomogeneity, $\gamma_{e_k g}$ is the electronic dephasing rate constant, and $\bar{n}_{kj} = 1/[\exp(\hbar\omega_{kj}/kT) - 1]$. Huang−Rhys factor S_{kj} is defined by $S_{kj} = \omega_{kj}/2\hbar(\Delta Q_{kj})^2$, where ΔQ_{kj} denotes the distance, along the jth normal coordinate, between the equilibrium positions of the potential surfaces of the electronic excited state e_k and electronic ground state g.

To investigate temperature dependence of the absorption spectra of RCs, determination of the electronic states and the vibrational modes of each electronic state is necessary. In particular, as can be seen from eq 2a, the electronic dipole transition moments $\{\vec{\mu}_{e_k g}\}$ will play an important role in constructing the total absorption band over which several electronic states are involved.

B. Hamiltonian for Electronic States. We consider a model for the electronic states of special pair and two Bchl monomers of the RC. Figure 1 illustrates the location and coupling scheme of these four Bchls. B_1 and B_2 denote Bchls in the M and L branches of special pair, respectively. Below B_1 (B_2) is the

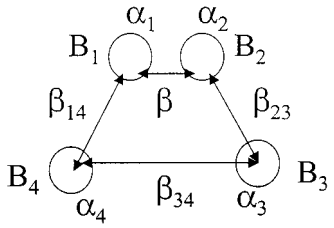

Figure 1. The 4-Bchl-interaction model. The electronic energy of every B_i is α_i, $i = 1-4$. The coupling between B_1 and B_2, B_1 and B_4, B_2 and B_3, and B_3 and B_4 are β, β_{14}, β_{23}, and β_{34}, respectively.

monomer Bchl indicated by B_4 (B_3). In Figure 1, α_1, α_2, α_3, and α_4 represent the energies of B_1, B_2, B_3, and B_4, respectively. We assume that these energies are different because the protein environment in the vicinity of each Bchl is different. In particular, α_1 and α_2 are quite different and we assume that these two energies are given by $\alpha_1 = \bar{\alpha} + \Delta$ and $\alpha_2 = \bar{\alpha} - \Delta$ where $\bar{\alpha}$ is the averaged energy of these two energies and Δ (>0) is the deviation from the average.

With the localized basis set, that is, $|\chi_l\rangle = |e_l\rangle\prod_{m\neq l}|g_m\rangle$ where $|e_l\rangle$ ($|g_m\rangle$) is the electronically excited (ground) state of the Bchl B_l (B_m), the total electronic Hamiltonian for the model system is given by

$$\mathbf{H} = \begin{pmatrix} \bar{\alpha}+\Delta & \beta & 0 & \beta_{14} \\ \beta & \bar{\alpha}-\Delta & \beta_{23} & 0 \\ 0 & \beta_{23} & \alpha_3 & \beta_{34} \\ \beta_{14} & 0 & \beta_{34} & \alpha_4 \end{pmatrix} \tag{3}$$

where β and β_{lm} represent the electronic coupling constant between the Bchls B_1 and B_2 and that between the Bchls B_l and B_m, respectively.

C. Delocalized Model. To diagonalize eq 3, one can adopt a delocalized basis set defined by

$$|e_k\rangle = \sum_{l=1}^{4} C_k^l |\chi_l\rangle \tag{4}$$

The electronic transition moment between $|e_k\rangle$ and $|g\rangle = |g_1\rangle|g_2\rangle|g_3\rangle|g_4\rangle$ is given by

$$\vec{\mu}_{e_k g} = \langle e_k| \sum_{l=1}^{4} \vec{\mu}(\mathrm{B}_l)|g\rangle = \sum_{l=1}^{4} C_k^l \langle\chi_l|\vec{\mu}_{\mathrm{B}_l}|g_l\rangle \tag{5}$$

The absorption intensity can then be expressed as the square of the transition moment. For example, the normalized intensity ratio of the second lowest to the lowest transition is given by

$$\frac{|\vec{\mu}_{e_1 g}|^2}{|\vec{\mu}_{e_2 g}|^2} = \frac{\sum_{l=1}^{4}\sum_{m=1}^{4} C_1^l C_1^m \cos\theta_{B_l B_m}}{\sum_{l=1}^{4}\sum_{m=1}^{4} C_2^l C_2^m \cos\theta_{B_l B_m}} \tag{6}$$

where $\theta_{\mathrm{B}_l\mathrm{B}_m}$ is the angle between the electronic transition dipole moments of the two Bchls B_l and B_m. In eq 6, we have assumed $|\vec{\mu}_{\mathrm{B}_1}| = |\vec{\mu}_{\mathrm{B}_2}| = |\vec{\mu}_{\mathrm{B}_3}| = |\vec{\mu}_{\mathrm{B}_4}| = |\vec{\mu}_{\mathrm{B}}|$ although the protein environment is different for each Bchl.

D. Dimer Model. For the case in which the magnitude of β is larger than that of any β_{lm} in eq 3, dimer basis set can be constructed. Notice that, in our model, the dimer does not consist of two identical Bchls. By taking into account Δ, our model considers a dimer comprising two electronically asymmetric Bchls.

We first define a unitary matrix as

$$\mathbf{U} = \begin{pmatrix} \cos\theta & -\sin\theta & 0 & 0 \\ \sin\theta & \cos\theta & 0 & 0 \\ 0 & 0 & 1 & 0 \\ 0 & 0 & 0 & 1 \end{pmatrix} \tag{7}$$

where

$$\tan\theta = \frac{\beta}{\alpha} \tag{8a}$$

and

$$\alpha = \Delta + \sqrt{\Delta^2 + \beta^2} \equiv \Delta + \Omega \tag{8b}$$

The unitary transformation applying eq 7 to eq 3 yields

$$\tilde{\mathbf{H}} = \mathbf{U}^{+}\mathbf{H}\mathbf{U} = \tilde{\mathbf{H}}_0 + \tilde{\mathbf{V}} \tag{9}$$

and

$$\tilde{\mathbf{H}}_0 = \begin{pmatrix} \bar{\alpha}+\Omega & 0 & 0 & 0 \\ 0 & \bar{\alpha}-\Omega & 0 & 0 \\ 0 & 0 & \alpha_3 & 0 \\ 0 & 0 & 0 & \alpha_4 \end{pmatrix} \tag{10a}$$

$$\tilde{\mathbf{V}} = \begin{pmatrix} 0 & 0 & \beta_{23}\sin\theta & \beta_{14}\cos\theta \\ 0 & 0 & \beta_{23}\cos\theta & -\beta_{14}\sin\theta \\ \beta_{23}\sin\theta & \beta_{23}\cos\theta & 0 & \beta_{34} \\ \beta_{14}\cos\theta & -\beta_{14}\sin\theta & \beta_{34} & 0 \end{pmatrix} \tag{10b}$$

The dimer basis set can be expressed as

$$|\mathrm{P}_+\rangle = \cos\theta|\chi_1\rangle + \sin\theta|\chi_2\rangle \tag{11a}$$

$$|\mathrm{P}_-\rangle = \sin\theta|\chi_1\rangle - \cos\theta|\chi_2\rangle \tag{11b}$$

$$|\mathrm{B}_3\rangle = |\chi_3\rangle \tag{11c}$$

and

$$|\mathrm{B}_4\rangle = |\chi_4\rangle \tag{11d}$$

In this case, the intensity ratio of the excitonic transitions becomes

$$\frac{|\vec{\mu}_{\mathrm{P}_{+g}}|^2}{|\vec{\mu}_{\mathrm{P}_{-g}}|^2} = \frac{1 + 2\cos\theta\sin\theta\cos\theta_{\mathrm{B}_1\mathrm{B}_2}}{1 - 2\cos\theta\sin\theta\cos\theta_{\mathrm{B}_1\mathrm{B}_2}} \tag{12}$$

Note that in the dimer model the absorption intensity depends on Δ and β.

III. Results and Discussion

A. Thermal Expansion Model. As mentioned in introduction, we have proposed a thermal expansion model to interpret the temperature-dependent peak shifts observed in the absorption spectra of R26 mutant RCs. In this model, the temperature dependence of the excitonic energy splitting $\Delta E = E_{\mathrm{P}_+} - E_{\mathrm{P}_-}$ is assumed to be mainly due to the chromophore dipole−dipole interaction; that is, since the chromophores are assumed to be fixed in a specific site of the protein, the thermal expansion of the protein environment affects this interaction. The nature of the excitonic energy splitting, in particular, involvement of CT states should be clarified from a more microscopic point of view

based on quantum chemistry calculations. However, such study requires a very accurate geometry of the electronic ground state of the RC including the protein residues and water molecules. We should note here that despite of computational difficulties, several extensive calculations have been performed to obtain a more accurate description of the electronic states of RCs.[59,65−69]

In the dipole−dipole interaction model, the energy gap $\Delta E = E_{P_+} - E_{P_-}$ is inversely proportional to R^3, that is,

$$\Delta E = K'/R^3 \tag{17a}$$

where K' is a constant independent of T and R is the distance between the dimer Bchls. In the thermal expansion model, we find $R = R_0\{1 + \xi(T - T_0)\}$ where ξ denotes the thermal expansion coefficient and T_0 is a reference temperature. It follows that

$$\Delta E = \frac{K'}{R_0^3}\frac{1}{\{1 + \xi(T - T_0)\}^3} \approx K_0\{1 - 3\xi(T - T_0)\} \tag{17b}$$

where K_0 is a constant depending on a reference temperature T_0.

B. Temperature-Dependent Band Shift of R26.Phe-a. In the previous paper, using eq 17, we obtained the values of K_0 and ξ for R26 RCs.[62] However, we did not associate these quantities with the microscopic properties of the dimer such as the electronic asymmetry Δ and the intra-dimer coupling β presented in the above section. In addition, the temperature-dependent absorption spectra of R26.Phe-a RCs[52] have not been analyzed using the expansion model so far. In this subsection, we focus on the R26.Phe-a mutant RCs because the absorption spectra of this mutant at various temperatures have been reported by Huber et al.[52] In the R26.Phe-a mutant RCs, the bacteriopheophytins are replaced by the plant pheophytins. Obviously, the H bands in the absorption spectra disappear at various temperatures. However, by comparing the spectra of this mutant with those of R26 at a few similar temperatures (R26.Phe-a at 50 K vs R26 at 77 K and R26.Phe-a at 295 K vs R26 at 298 K), the peak positions of the P and B bands of these two mutants are found to be very close and the shapes are very similar to each other. This indicates that the plant pheophytins have weak interactions with the four Bchls. Thus, effects of the plant pheophytins on the electronic states and absorption spectra of R26.Phe-a RCs will not be considered here.

B.1. Dimer Description. To construct the electronic Hamiltonian given by eq 10, Δ and β should be associated with temperature and ξ. In addition, the values of $\bar{\alpha}$, β_{13}, β_{24}, and β_{34} should be determined. First, as a coarse estimation, we shall determine Δ, β, and ξ using the dimer model. For this purpose, we analyze the temperature dependence energy gap between $|P_+\rangle$ and $|P_-\rangle$. In the dimer model, the gap can be expressed, using eq 10a, as

$$\Delta E = E_{P_+} - E_{P_-} = 2\Omega = 2\sqrt{\Delta^2 + \beta^2} \tag{18}$$

In the thermal expansion model, we find

$$\Omega(T) = \frac{\Delta E(T)}{2} = \Omega_0[1 - 3\xi(T - T_0)] \tag{19}$$

where Ω_0 is the half of the energy gap $\Delta E(T_0)$ at a reference temperature T_0. From eqs 18 and 19, we find that $\Omega_0\{1 - 3\xi(T - T_0)\} = \sqrt{\Delta^2+\beta^2}$. In other words, the microscopic quantities Δ and β depend on temperature. Although there are several possible mechanisms that associate Δ and β with temperature,

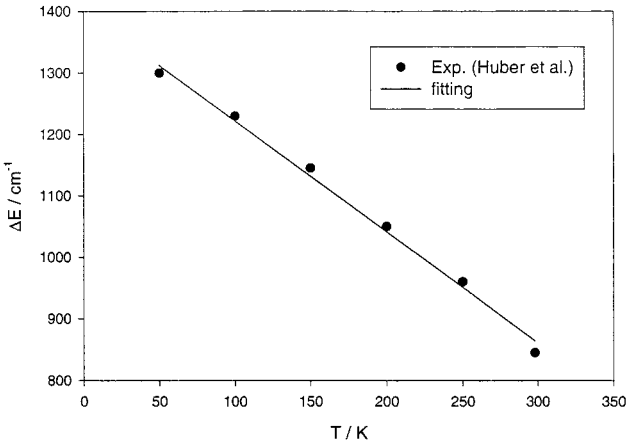

Figure 2. The temperature dependence of the energy differences between the 0−0 transitions of the P_+ and P_- band. Solid line is the fitting result by using the thermal expansion model.

TABLE 2: Expansion Coefficients ξ of Some Solvents[70]

solvent	$\xi/(10^{-4}\ K^{-1})$
CCl_4	12.4
EtOH	11.2
H_2O	2.1
C_6H_6	12.4

we shall propose

$$\Delta(T) = \Delta_0[1 - 3\xi(T - T_0)] \tag{20}$$

and

$$\beta(T) = \beta_0[1 - 3\xi(T - T_0)] \tag{21}$$

as the first step to understand the temperature-dependent absorption spectra of RCs. Of course, a more detailed mechanism should be investigated to clarify how structural rearrangements induced due to T affect these quantities.

The energy gaps of R26.Phe-a mutant RCs at 50, 100, 150, 200, 250, and 295 K are available as listed in Table 1. First we apply eq 19 to obtain Ω_0 and ξ for this mutant using nonlinear fitting algorithm and setting $T_0 = 50$ K as a reference temperature. Figure 2 shows the fitting result: Ω_0 and ξ are obtained to be 656.06 cm^{-1} and 4.67 $\times$ 10^{-4}/K, respectively. For comparison, Table 2 presents the thermal expansion coefficients of several solvents.[70] From Table 2, we can see that the ξ value is quite reasonable.

Recently, Scherer et al. have used the dimer model to interpret experimental results of their time-resolved anisotropy measurements.[53] According to them, the ratio of the transition dipole strengths is expressed as

$$\frac{|\vec{\mu}_{P_+g}|^2}{|\vec{\mu}_{P_-g}|^2} = \frac{1 + \sin\varphi\cos\theta_{B_1B_2}}{1 - \sin\varphi\cos\theta_{B_1B_2}} \tag{22}$$

where $\theta_{B_1B_2}$ is the angle between the Q_y transition moments of the two monomer Bchls in the special pair. Note that $\varphi = 2\theta$ where θ is given in eq 8a. The anisotropy analysis implied that $\varphi \cong 70°$, $|\vec{\mu}_{P_+g}|^2/|\vec{\mu}_{P_-g}|^2 = 1/10$, and $E_{B_1} - E_{B_2} = 294$ cm^{-1}.

In the dimer model (eq 10a), $E_{B_1} - E_{B_2}$ is associated with 2Δ. Thus, from $E_{B_1} - E_{B_2} = 294$ cm^{-1}, we find that Δ at room temperature is given by 147 cm^{-1}. In this case, using eqs 20 and 21, the Δ_0 and β_0 can be calculated to be 223.7 cm^{-1} and 616.7 cm^{-1}, respectively.

TABLE 3: The Temperature Dependence of the Angle Relation, Transition Dipole Strength Ratio, and Transition Dipole Orientation of the Chromophores in the R26.Phe-a RCs

T/K	295	250	200	150	100	50	15
$\theta_{B_1B_2}$ [a]	146.54	141	131.26	130	127.17	124.22	123.1
θ_{B_3} [b]	68	68	68	68	68	68	68
θ_{B_4} [b]	66	66	66	66	66	66	66
			Transition Dipole Strength Ratio				
(1) $\lvert\vec{\mu}_{e_1g}\rvert^2/\lvert\vec{\mu}_{e_2g}\rvert^2$	0.096	0.129	0.204	0.213	0.239	0.270	0.287
(2) $\lvert\vec{\mu}_{e_3g}\rvert^2/\lvert\vec{\mu}_{e_2g}\rvert^2$	0.610	0.624	0.656	0.657	0.661	0.658	0.643
(3) $\lvert\vec{\mu}_{e_4g}\rvert^2/\lvert\vec{\mu}_{e_2g}\rvert^2$	0.497	0.517	0.559	0.570	0.592	0.619	0.638
(2) + (3)	1.107	1.141	1.215	1.227	1.253	1.277	1.281
			Transition Dipole Orientation				
$\vec{\mu}_{e_1g}\cdot\vec{\mu}_{e_2g}$	−0.230	−0.2053	−0.1566	−0.1412	−0.1136	−0.0764	−0.0438

[a] Angles (degrees) between the transition moments of the special pair dimer. [b] Angles of the transition moments with the membrane normal.

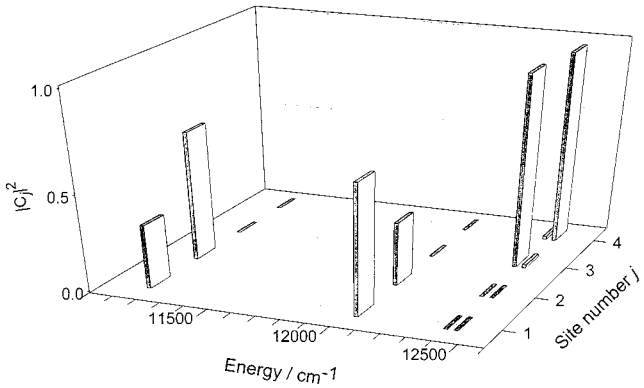

Figure 3. The site contribution of the wave functions of the states for the delocalized model at 295 K.

B.2. Delocalized Electronic States. We shall generalize the results obtained based on the dimer model and apply them to construct delocalized electronic states and their energies. For this purpose, we apply eqs 20 and 21 and the obtained values $\Delta_0 = 223.7\ cm^{-1}$, $\beta_0 = 616.7\ cm^{-1}$, and $\xi = 656.06\ cm^{-1}$ to eq 3. The values of $\bar{\alpha}$, β_{13}, β_{24}, and β_{34} in eq 3 are still needed to be determined. $\bar{\alpha}$ should be the middle value of the 0−0 transitions of the P_+ and P_- bands, thus we set $\bar{\alpha}$ value as 11625 cm^{-1}. Moreover, we set α_3 and α_4 values as 12403 and 12500 cm^{-1}. The values of β_{13}, β_{24}, and β_{34} can be adopted from the literature,[71,72] and they are given by 20, 30, and 10 cm^{-1}, respectively. Note that we assume that β_{13}, β_{24}, and β_{34} values are independent of temperature. This assumption is reasonable since the distances of $B_1 - B_3$, $B_2 - B_4$, and $B_3 - B_4$ are much larger that of $B_1 - B_2$ so that distance changes due to thermal expansion should be ignored.

Diagonalizing eq 3, the eigen energies and the corresponding wave functions can be calculated. Figure 3 shows the calculated site contribution defined by $|\langle\chi_l|e_k\rangle|^2$ where l denotes the site number presented in Figure 1 and $|e_k\rangle$ is the wave function of kth electronic state. In Figure 3, $|\langle\chi_l|e_k\rangle|^2$ at room temperature is presented. One can see asymmetrical contributions of B_1 and B_2 in the lowest and second lowest energy states. This situation may be associated with asymmetrical charge distribution of the special pair observed in EPR spectra.[73]

To verify our generalization for applying the dimer values to eq 3, we calculate the second-order energies $E^{(2)}$ (see Appendix A, eq A2d) and find that the second order correction is very small compared with $E^{(0)}$ (eq A2a) for all the states and all the temperature range. That is, the energy differences $E_{P_+} - E_{P_-}$ in Table 1 can be approximately equal to the 2Ω values (errors within a few percentages). Therefore, our generalization is reasonable.

B.3. Band Intensity Ratio and Absorption Spectra. According to eqs 1 and 2, to calculate absorption spectra of multielectronic states, the transition dipole moment squares are needed for all the electronic states involved in the relevant optical transition. For this purpose, we next discuss the configurations of the transition dipole moments of the chromophores.

As mentioned above, Scherer et al. have reported that the angle φ is about 70° which leads to $\theta = 35°$ and the ratio of the excitonic transition intensity of P_+ to that of P_- is 1/10. Calculated using eq 22, the angle θ (i.e., $\theta_{B_1B_2}$ in eq 12) between the transition moments of B_1 and B_2 is given by 150.54° at room temperature. As far as we know, no reports have been made to other temperature cases so far.

Equation 6 indicates that for the delocalized model, the transition dipole intensity ratio is related to $\theta_{B_jB_m}$. To obtain $\theta_{B_jB_m}$ at various temperatures, we utilize Breton's data[74] regarding the angles between the electronic transition moments of the 4 BChls and the normal axis of the membrane (see Appendix B for detail). The calculated $\theta_{B_jB_m}$ are listed in Table 3.

By using eq 6 and applying $\theta_{B_1B_2}$ (Table 3) and the wave function coefficients of the delocalized model at various temperatures to calculate the peak ratios $|\vec{\mu}_{e_1g}|^2/|\vec{\mu}_{e_2g}|^2$, $|\vec{\mu}_{e_3g}|^2/|\vec{\mu}_{e_2g}|^2$, and $|\vec{\mu}_{e_4g}|^2/|\vec{\mu}_{e_2g}|^2$, they are found to simultaneously agree with the values presented in Table 1. Table 3 lists the calculation results of the delocalized model, including the angles between any two Bchls and the transition dipole moment intensity ratios $|\vec{\mu}_{e_1g}|^2/|\vec{\mu}_{e_2g}|^2$, $|\vec{\mu}_{e_3g}|^2/|\vec{\mu}_{e_2g}|^2$, and $|\vec{\mu}_{e_4g}|^2/|\vec{\mu}_{e_2g}|^2$ at various temperatures. Additionally, the inner products of $\vec{\mu}_{e_1g}$ and $\vec{\mu}_{e_2g}$, namely, $(\vec{\mu}_{e_1g}\cdot\vec{\mu}_{e_2g})$, are also presented in this Table 3. The inner product $(\vec{\mu}_{e_1g}\cdot\vec{\mu}_{e_2g})$ can be given by

$$(\vec{\mu}_{e_1g}\cdot\vec{\mu}_{e_2g}) = \sum_{l=1}^{4}\sum_{m=1}^{4} C_1^l\, C_2^m(\vec{\mu}_{B_l}\cdot\vec{\mu}_{B_m}) \cong |\vec{\mu}_B|^2 \sum_{l=1}^{4}\sum_{m=1}^{4} C_1^l\, C_2^m \cos\theta_{B_lB_m} \quad (23)$$

Because $\vec{\mu}_{e_1g}\cdot\vec{\mu}_{e_2g}$ is not equal to zero in Table 3, $\vec{\mu}_{e_1g}$ is not perpendicular to $\vec{\mu}_{e_2g}$.[21,39] This situation is also reported by Hochstrasser and Scherer.[51,53]

Note that both the delocalized and dimer models can be used to explain temperature dependence of the absorption spectra of R26.Phe-a RCs. This is due to the fact that the interactions (eq 10b) among Bchls, except for the interaction between B_1 and B_2, are small compared with the diagonal element Hamiltonian in eq 10a.

Now we are in a position to calculate the absorption coefficient with displaced harmonic potential surfaces using eq 2. Substituting the electronic and vibrational properties listed in Tables 3 and Table 4[61,62] into eq 2 and applying fast Fourier

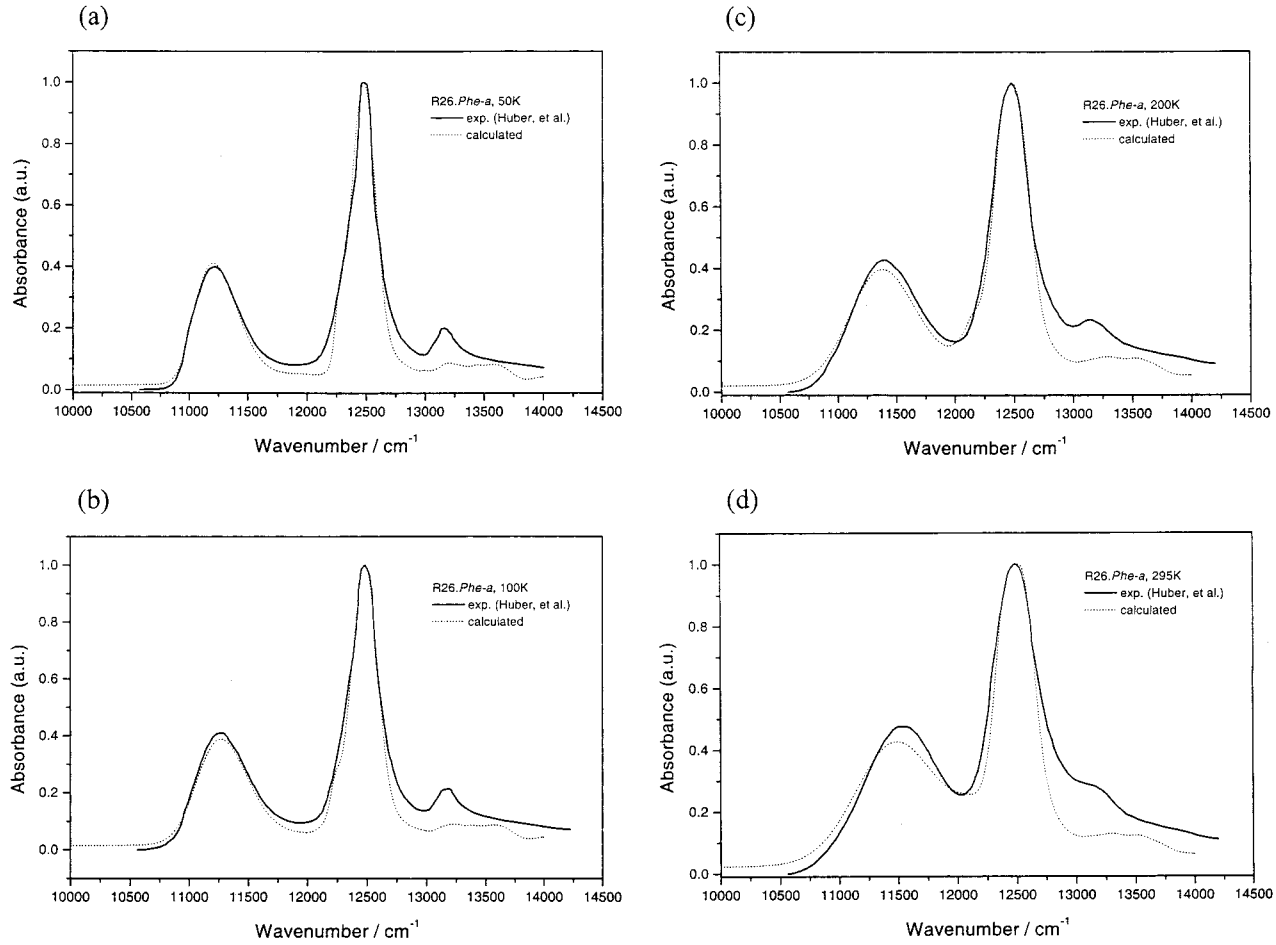

Figure 4. The absorption spectra of the R26.Phe-a RCs at various temperatures. The experimental data taken from Huber et al.[51] and the absorption spectra calculated by using the electronic structures and interactions presented in the text and the vibrational properties adopted from the previous work.[61,62]

TABLE 4: Selected Vibrational Frequencies, Huang−Rhys Factors, and Electronic Energy Levels of the Involved States of RCs of *Rb. Sphaeroides*

	vibrational modes							
ω_j/S$_j$	34	128	224	560	730	1160	1400	1520
P_-^*	2.200	1.600	0.045	0.017	0.033	0.030	0.020	0.040
P_+^*	0.160	0.570	0.045	0.017	0.033	0.030	0.020	0.040
B_1^*	0.800	0.079	0.083	0.032	0.070	0.001	0.064	0.040
B_2^*	0.800	0.079	0.083	0.032	0.070	0.001	0.064	0.040

transform (FFT) method to eq 2, we simulate absorption spectra of the R26.Phe-a RC at various temperatures. The FFT was performed using 32768 points with a time step of 3.0517 × 10^5 cm, which leads to 1 cm^{-1} resolution in the transformed frequency domain. Figure 4 compares the experimental absorption spectra at various temperatures with the corresponding calculated absorption spectra using the delocalized model with the thermal expansion model. One can see good agreement between the experimental and theoretical spectra at all temperatures. As theoretical prediction, we also simulate the absorption spectra of R26.Phe-a RCs at 77 and 278 K in Figure 5.

C. Anisotropy of R26.Phe-a. To study the difference between these two models, we calculate the anisotropy of several pairs of two electronic transitions by using

$$r(e_k,e_{k'}) = \frac{3(\vec{\mu}_{e_kg}\cdot\vec{\mu}_{e_{k'}g})^2 - (\vec{\mu}_{e_kg}\cdot\vec{\mu}_{e_kg})(\vec{\mu}_{e_{k'}g}\cdot\vec{\mu}_{e_{k'}g})}{(\vec{\mu}_{e_kg}\cdot\vec{\mu}_{e_kg})(\vec{\mu}_{e_{k'}g}\cdot\vec{\mu}_{e_{k'}g})} \quad (24)$$

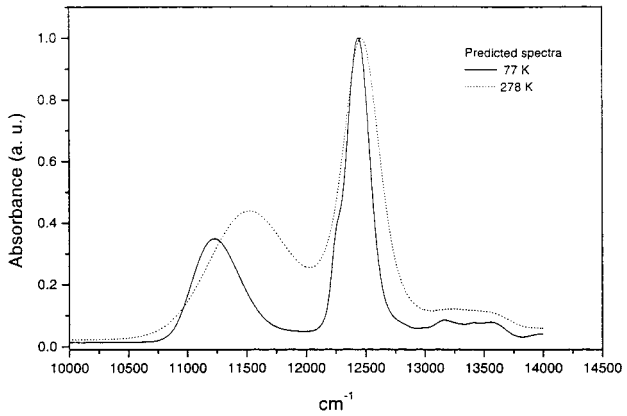

Figure 5. The predicted absorption spectra at 77 and 278 K. The peak positions and intensities are based on the thermal expansion model (Table 3); vibrational information are according to Table 4.

We calculate three models: (1) the dimer model presented in this work, (2) the dimer model employed by Scherer et al., and (3) the delocalized model. Table 5 lists the calculated results as a function of temperature. The anisotropy values for $r(e_1,e_2)$ at 295 K are found to be quite different between the dimer and delocalized models. The difference is about 53%. Meanwhile, the differences at other temperatures are within about 13−14%. For $r(e_2,e_3)$, the differences are within 24−28%. Table 5 also lists the angle between B_1 and B_2 in the special pair of R26.Phe-a RCs as a function of temperature.

TABLE 5: The Anisotropy between the Transition Dipole Moments of the Chromophores in the Dimer Model and Delocalized Model[a]

	model	295 K	200 K	100 K	50 K
$r_{B_1B_2}$	dimer	−0.040	−0.141	−0.152	−0.160
	dimer[b]	−0.039			
	delocalized	−0.085	−0.163	−0.176	−0.185
$r_{B_2B_3}$	dimer	−0.096	−0.083	−0.080	−0.077
	delocalized	−0.127	−0.115	−0.110	−0.106
$\theta_{B_1B_2}$	dimer	150.50	134.11	131.01	127.98
	delocalized	146.54	131.26	127.17	124.22

[a] The angle between $\vec{\mu}_{e_1g}$ and $\vec{\mu}_{e_2g}$ in different model also shown for comparison. [b] From ref 53.

It should be noted that the calculated anisotropy may not be applied to femtosecond time-resolved anisotropy measurements because femtosecond time-resolved experiments involve pumping and probing conditions and may involve overlapping overlap between the vibronic structures of several electronic states due to the use of femtosecond laser pulses. Nevertheless, we think the calculated anisotropy using eq 24 can provide a reference in comparing models.

As mentioned in the previous section, the temperature-dependent absorption spectra of RCs are very important for the understanding of the molecular properties such as the electronic configurations, vibrational contributions, and transition moment relations of the Bchls in RCs. However, only in the R26.Phe-a mutant case have absorption spectra at various temperatures so far been available. Although the absorption spectra of the WT and R26 mutant RCs are available at a few temperatures like 1, 4, 77, and 298 K,[39,40,42,44,53] the analyzed results are not so consistent (see Table 1). It may be because the preparation methods of RCs and the experimental conditions are somewhat different for different groups. Thus, to examine validity of the electronic state model and the thermal expansion model presented in this work, absorption spectra experiments of each RC at various temperatures should be carefully performed.

IV. Conclusion

Detailed analysis of the absorption spectra of the R26.Phe-a mutant RCs at various temperatures has been presented constructing a model Hamiltonian based on the previous spectral analysis results. The temperature dependence of the electronic asymmetry and the coupling between the Bchls in the special pair can be obtained by using the thermal expansion model. In the thermal expansion model, we have proposed that the electronic asymmetry and the coupling between the Bchls in the special pair are linearly dependent on temperature (ref 75). The mechanism of the temperature-dependent P band peak shift appearing in the absorption spectra of RCs can be interpreted by this model.

The delocalized basis set is constructed numerically in this work. Using the second-order perturbation method, the delocalized basis set can also be constructed because the interactions among chromophores except for two Bchls in the special pair are quite small compared with the zero-th order Hamiltonian (see Appendix A). The differences between the calculated results via the numerical method and the perturbation method are within 2.5%.

After optimizing the angles between the transition moments of the special pair components, the transition intensity ratios of the chromophores are calculated and these values agree with the previous data at various temperatures listed in Table 1. The absorption spectra of R26.Phe-a mutant RCs at various temperatures have been reconstructed and the calculated results show good agreement with the experiment reported by Huber et al. The absorption spectra at 77 and 278 K have been theoretically predicted by using the model presented in this paper.

To consider the difference between the dimer and delocalized models, the anisotropy values among a few electronic transitions are also calculated using a very simplified equation. The most obvious difference is that the anisotropy values of the first and second electronic transitions at 295 K are found to be quite different between the dimer and delocalized models. Meanwhile, the differences between the anisotropy values of the first and third electronic transitions using these two models are found to be within 22−28% at several temperatures including 295 K.

This work focuses on R26.Phe-a mutant RCs because the absorption spectra at various temperatures have been available for only this mutant so far. Other mutants of *Rb. sphaeroides*, including WT, can be analyzed in similar fashion presented in this paper if experimental absorption spectra at various temperatures are available.

Appendix A. Perturbation Method Calculation

For the case in which the matrix elements in eq 10b are smaller than those of any diagonal energy differences, perturbation theory can be applied to construct a delocalized basis set from the dimer basis set. In this case, the energy correction to the second order can be given by

$$\mathbf{E} = \mathbf{E}^{(0)} + \mathbf{E}^{(2)} \tag{A1}$$

where

$$\mathbf{E}^{(0)} = \begin{pmatrix} \bar{\alpha} + \Omega & 0 & 0 & 0 \\ 0 & \bar{\alpha} - \Omega & 0 & 0 \\ 0 & 0 & \alpha_3 & 0 \\ 0 & 0 & 0 & \alpha_4 \end{pmatrix} \tag{A2a}$$

$$\mathbf{E}^{(2)} = \begin{pmatrix} \sum_{l\neq 1} \frac{\tilde{V}_{1l}\tilde{V}_{l1}}{E_1^{(0)} - E_l^{(0)}} & 0 & 0 & 0 \\ 0 & \sum_{l\neq 2} \frac{\tilde{V}_{2l}\tilde{V}_{l2}}{E_2^{(0)} - E_l^{(0)}} & 0 & 0 \\ 0 & 0 & \sum_{l\neq 3} \frac{\tilde{V}_{3l}\tilde{V}_{l3}}{E_3^{(0)} - E_i^{(0)}} & 0 \\ 0 & 0 & 0 & \sum_{l\neq 4} \frac{\tilde{V}_{4l}\tilde{V}_{l4}}{E_4^{(0)} - E_l^{(0)}} \end{pmatrix} \tag{A2b}$$

and

$$\tilde{V}_{kl} = \langle \chi_k | \tilde{V} | \chi_l \rangle \tag{A2c}$$

The corresponding wave functions (delocalized basis set) can be expressed as

$$|e_k\rangle \approx |e_k\rangle^{(0)} + |e_k\rangle^{(1)} + |e_k\rangle^{(2)}, \qquad k = 1,...,4 \tag{A3}$$

where

$$|e_1\rangle^{(0)} = |P_+\rangle,\ |e_2\rangle^{(0)} = |P_-\rangle,\ |e_3\rangle^{(0)} = |\chi_3\rangle,\ |e_4\rangle^{(0)} = |\chi_4\rangle$$

$$|e_k\rangle^{(1)} = \sum_{l\neq k}^{4} a_{kl}^{(1)}|e_l\rangle^{(0)} \tag{A4a}$$

$$|e_k\rangle^{(2)} = -\frac{1}{2}\sum_{l\neq k}|a_{kl}^{(1)}|^2|e_l\rangle^{(0)} + \sum_{m\neq K}\sum_{l\neq K}\frac{{}^{(0)}\langle\chi_k|\tilde{V}|\chi_m\rangle^{(0)(0)}\langle\chi_m|\tilde{V}|e_l\rangle^{(0)}}{(E_k - E_m)(E_k - E_l)}|e_l\rangle^{(0)} \tag{A4b}$$

and

$$a_{kl}^{(1)} = \frac{\langle\chi_k|\tilde{V}|\chi_l\rangle}{E_K - E_l} \tag{A4c}$$

Appendix B. Determination of $\theta_{B_1B_2}$

To obtain a coarse estimation of $\theta_{B_1B_2}$ for the R26.Phe-a mutant RCs at various temperatures, we first use eq 12. The $|\vec{\mu}_{P_+g}|^2/|\vec{\mu}_{P_-g}|^2$ in eq 12 can be given by the peak ratio of P_+ to P_- at each temperature in Table 1. Substituting these values into eq 12 yields different $\theta_{B_1B_2}$ values at different temperatures. These $\theta_{B_1B_2}$ values are combined with Breton's data[64] regarding the angles between the transition moments of the 4 Bchls and the normal axis of the membrane. If substituting these angles and $\theta = \tan^{-1}(\alpha/\beta)$ into eq 6, the intensity ratios deviate from Table 1 for all the temperature cases. This is due to the fact that the angles $\theta_{B_1B_2}$ obtained from eq 12; namely, the calculation of the dimer exciton model is just for a rough estimation of $\theta_{B_1B_2}$. If we reduce the $\theta_{B_1B_2}$ by 4° for these four temperature cases, e.g., for 295 K, 150.54° reduce to 146.54°; for 200 K, 135.26° to 131.26°, etc. The calculated peak ratios show good agreement with the values listed in Table 1.

Note Added in Proof. In this work, we have neglected a higher order multiple interactions[75] in the thermal expansion model for the energy gap. These interactions can be incorporated, for example, in the following form:

$$\Delta E = \sum_{n=3}\frac{K^{(n)}}{R^n}$$

and in the thermal expansion model, it follows that

$$\Delta E = \sum_{n=3}\frac{K^{(n)}}{R_0^n} - \xi(T - T_0)\sum_{n=3} n\frac{K^{(n)}}{R_0^n}$$

where the term of $n=3$ corresponds to eq 17b. The effect of these higher order terms on ΔE will be investigated in future work.

Acknowledgment. This work was supported by the National Science Council of ROC and Academia Sinica. CHC is grateful to the referees for their useful comments and suggestions.

References and Notes

(1) Martin, J.-L.; Breton, J.; Hoff, A. J.; Migus, A.; Antonetti, A. *Proc. Natl. Acad. Sci. U.S.A.* **1986**, *83*, 857.
(2) Fleming, G. R.; Martin, J.-L.; Breton, J. *Nature* **1988**, *333*, 190.
(3) Breton, J.; Martin, J.-L.; Fleming, G. R.; Lambry, J.-C. *Biochemistry* **1988**, *27*, 8276.
(4) Vos, M. H.; Lambry, J.-C.; Robles, S. J.; Breton, J.; Martin, J.-L. *Proc. Natl. Acad. Sci. U.S.A.* **1992**, *89*, 613.
(5) Vos, M. H.; Jones, M. R.; Hunter, C. N.; Breton, J.; Lambry, J.-C.; Martin, J.-L. *Biochemistry* **1994**, *33*, 6750.
(6) Chan, C.-K.; Chen, L. X.-Q.; DiMagno, T. J.; Hanson, D. K.; Nance, S. L.; Schiffer, M.; Norris, J. R.; Fleming, G. R. *Chem. Phys. Lett.* **1991**, *176*, 366.
(7) Du, M.; Rosenthal, S. J.; Xie, X.; DiMagno, T. J.; Schmidt, M.; Hanson, D. K.; Schiffer, M.; Norris, J. R.; Fleming, G. R. *Proc. Natl. Acad. Sci. U.S.A.* **1992**, *89*, 8517.
(8) Jia, Y.; Jones, D. M.; Joo, T.; Nagasawa, Y.; Lang, M. J.; Fleming, G. R. *J. Phys. Chem.* **1995**, *99*, 6263.
(9) Groot, M.-L.; Yu, J.-Y.; Agarwal, R.; Norris, J. R.; Fleming, G. R. *J. Phys. Chem.* **1998**, *102*, 5923.
(10) Walker, G. C.; Maiti, S.; Cowen, B. R.; Moser, C. C.; Dutton, P. L.; Hochstrasser, R. M. *J. Phys. Chem.* **1994**, *98*, 5778.
(11) Breton, J.; Martin, J.-L.; Migus, A.; Antonetti, A.; Orszag, A. *Proc. Natl. Acad. Sci. U.S.A.* **1986**, *83*, 5121.
(12) Woodbury, N. W.; Becker, M.; Middendorf, D.; Person, W. W. *Biochemistry* **1985**, *24*, 7516.
(13) Kirmaier, C.; Holten, D. *Proc. Natl. Acad. Sci. U.S.A.* **1990**, *87*, 3552.
(14) Vos, M. H.; Lambry, J.-C.; Robles, S. J.; Breton, J.; Martin, J.-L. *Proc. Natl. Acad. Sci. U.S.A.* **1991**, *88*, 8888.
(15) Vos, M. H.; Rappaport, F.; Lambry, J.-C.; Breton, J.; Martin, J.-L. *Nature* **1993**, *363*, 320.
(16) Vos, M. H.; Breton, J.; Martin, J.-L. *J. Phys. Chem. B* **1997**, *101*, 9820.
(17) Chan, C.-K.; DiMagno, T. J.; Chen, L. X.-Q.; Norris, J. R.; Fleming, G. R. *Proc. Natl. Acad. Sci. U.S.A.* **1991**, *88*, 11202.
(18) Wang, Z.; Pearlstein, R. M.; Jia, Y.; Fleming, G. R.; Norris, J. R. *Chem. Phys.* **1993**, *176*, 421.
(19) Jones, D. M.; Lang, M. J.; Nagasawa, Y.; Joo, T.; Fleming, G. R. *J. Chem. Phys.* **1996**, *100*, 12660.
(20) Maiti, S.; Walker, G. C.; Cowen, B. R.; Pippenger, R.; Moser, C. C.; Dutton, P. L.; Hochstrasser, R. M. *Proc. Natl. Acad. Sci. U.S.A.* **1994**, *91*, 10360.
(21) Chekalin, S. V.; Matveetz, Y. A.; Shkuropatov, A. Y.; Shuvalov, V. A.; Yartzev, A. P. *FEBS Lett.* **1987**, *216*, 245.
(22) Dressler, K.; Umlauf, E.; Schmidt, S.; Hamm, P.; Zinth, W.; Buchanan, S.; Michel, H. *Chem. Phys. Lett.* **1991**, *183*, 270.
(23) Schmidt, S.; Arlt, T.; Hamm, P.; Huber, H.; Nägele, T.; Wachtveil, J.; Meyer, M.; Scheer, H.; Zinth, W. *Chem. Phys. Lett.* **1994**, *223*, 116.
(24) Hamm, P.; Zinth, W. *J. Phys. Chem.* **1995**, *99*, 13537.
(25) van Stokkun, I. H. M.; Beekman, L. M.; Jones, M. R.; van Brederode, M. E.; van Grondelle, R. *Biochemistry* **1997**, *36*, 11360.
(26) van Brederode, M. E.; Jones, M. R.; van Grondelle, R. *Chem. Phys. Lett.* **1997**, *268*, 143.
(27) Streltsov, A. M.; Aartsma, T. J.; Hoff, A. J.; Shuvalov, V. A. *Chem. Phys. Lett.* **1997**, *266*, 347.
(28) Spörlein, S.; Zinth, W.; Wachtveitl, J. *J. Phys. Chem. B* **1998**, *102*, 7492.
(29) Lewis, J. W.; Goldback, R. A.; Kliger, D. S.; Xie, X.; Dunn, R. C.; Simon, J. D. *J. Phys. Chem.* **1992**, *96*, 5243.
(30) Cherepy, N. J.; Shreve, A. P.; Moore, L. J.; Boxer, S. G.; Mathies, R. A. *Proc. Natl. Acad. Sci. U.S.A.* **1991**, *88*, 11207.
(31) Wynne, K.; Haran, G.; Reid, G. D.; Moser, C. C.; Dutton, P. L.; Hochstrasser, R. M. *J. Phys. Chem.* **1996**, *100*, 5140.
(32) Holzapfel, W.; Finkele, U.; Kaiser, W.; Oesterhelt, D.; Scheer, H.; Stilz, H. U.; Zinth, W. *Proc. Natl. Acad. Sci. U.S.A.* **1990**, *87*, 5168.
(33) Arlt, T.; Schmidt, S.; Kaiser, W.; Lauterwasser, C.; Meyer, M.; Scheer, H.; Zinth, W. *Proc. Natl. Acad. Sci. U.S.A.* **1993**, *90*, 11757.
(34) Hamm, P.; Zurek, M.; Mäntele, W.; Meyer, M.; Scheer, H.; Zinth, W. *Proc. Natl. Acad. Sci. U.S.A.* **1995**, *92*, 1826.
(35) Zinth, W.; Arlt, T.; Wachtveitl, J. *Ber. Bunsen-Ges. Phys. Chem.* **1996**, *100*, 1962.
(36) van Brederode, M. E.; Jones, M. R.; van Mourik, F.; van Stokkun, I. H. M.; van Grondelle, R. *Biochemistry* **1997**, *36*, 6856.
(37) Stanley, R. J.; King, B.; Boxer, S. G. *J. Phys. Chem.* **1996**, *100*, 12052.
(38) Streltsov, A. M.; Vulto, S. I. E.; Ya, A.; Shkuropatov,; Hoff, A. J.; Aartsma, T. J.; Shuvalov, V. A. *J. Phys. Chem. B* **1998**, *102*, 7293.
(39) Steffen, M. A.; Lao, K.; Boxer, S. G. *Science* **1994**, *264*, 810.
(40) Hartwich, G.; Lossau, H.; Ogrodnik, A.; Michel-Beyerle, M. E. In *The Reaction Center of Photosynthetic Bacteria*; Michel-Beyerle, M. E., Ed.; Springer-Verlag: Berlin, 1996; pp 199.
(41) Cherepy, N. J.; Holzwarth, A. R.; Mathies, R. A. *Biochemistry* **1995**, *34*, 5288.
(42) Cherepy, N. J.; Shreve, A. P.; Moore, L. J.; Boxer, S. G.; Mathies, R. A. *J. Phys. Chem. B* **1997**, *101*, 3250.
(43) Reddy, N. R. S.; Lyle, P. A.; Small, G. J. *Photosynth. Res* **1992**, *31*, 167.
(44) Reddy, N. R. S.; Kolaczkowski, S. V.; Small, G. J. *J. Phys. Chem.* **1993**, *97*, 6934.

(45) Reddy, N. R. S.; Kolaczkowski, S. V.; Small, G. J. *Science* **1993**, *260*, 68.
(46) Cherepy, N. J.; Shreve, A. P.; Moore, L. J.; Boxer, S. G.; Mathies, R. A. *J. Phys. Chem.* **1994**, *98*, 6023.
(47) Cherepy, N. J.; Shreve, A. P.; Moore, L. J.; Boxer, S. G.; Mathies, R. A. *Biochemistry* **1997**, *36*, 8559.
(48) Johnson, S. G.; Tang, D.; Jankowiak, R.; Hayes, J. M.; Small, G. J. *J. Phys. Chem.* **1990**, *94*, 5849.
(49) Small, G. J.; Hayes, J. M.; Sillbey, R. J. *J. Phys. Chem.* **1992**, *96*, 7499.
(50) Lyle, P. A.; Kolaczkowski, S. V.; Small, G. J. *J. Phys. Chem.* **1993**, *97*, 6924.
(51) Haran, G.; Wynne, K.; Moser, C. C.; Dutton, P. L.; Hochstrasser, R. M. *J. Phys. Chem.* **1996**, *100*, 5562.
(52) Huber, H.; Meyer, M.; Scheer, H.; Zinth, W.; Wachveitl, J. *Photosynth. Res.* **1998**, *55*, 153.
(53) Arnett, D. C.; Moser, C. C.; Dutton, P. L.; Scherer, N. F. *J. Phys. Chem. B* **1999**, *103*, 2014.
(54) Parson, W. W.; Warshel, A. *J. Am. Chem. Soc.* **1987**, *109*, 6143.
(55) Parson, W. W.; Warshel, A. *J. Am. Chem. Soc.* **1987**, *109*, 6152.
(56) Boxer, S. G.; Goldstein, R. A.; Lockhart, D. J.; Midden-dorf, T. R.; Takiff, L. *J. Phys. Chem.* **1989**, *93*, 8280.
(57) Thompson, M. A.; Zerner, M. C. *J. Am. Chem. Soc.* **1991**, *113*, 8210.
(58) Thompson, M. A.; Zerner, M. C.; Fajer, J. *J. Phys. Chem.* **1991**, *95*, 5693.
(59) Small, G. J. *Chem. Phys.* **1995**, *197*, 239.
(60) Moore, L. J.; Zhou, H.; Boxer, S. G. *Biochemistry* **1999**, *38*, 10949.
(61) Chang, C. H.; Hayashi, M.; Chang, R.; Liang, K. K.; Yang, T.-S.; Lin, S. H. *Trends Chem. Phys.* **1999**, *7*, 247.
(62) Chang, C. H.; Hayashi, M.; Chang, R.; Liang, K. K.; Yang, T.-S.; Lin, S. H. *J. Chin. Chem. Soc.* **2000**, *47*, 785.
(63) Eyring, H.; Lin, S. H.; Lin, S. M. *Basic Chemical Kinetics*; Wiley-Interscience: New York, 1980.
(64) Lin, S. H.; Hayashi, M.; Alden, R. G.; Suzuki, S.; Gu, X.; Lin, Y. Y. In *Femtosecond Chemistry*; Mantz, J., Wöste, L., Ed.; VCH: New York, 1995; pp 633.
(65) Scherer, P. O. J.; Fischer, S. F. In *The Photosynthetic Bacterial Reaction Center II*; Breton, J., Verméglio, A., Eds.; NATO ASI Series 237; Plenum: New York, 1992; p 193.
(66) Warshel, A.; Chu, Z. T.; Parson, W. W. *J. Photochem. Photobiol. A* **1994**, *82*, 123.
(67) Gehlen, J. N.; Marchi, M.; Chandler, D. *Science* **1994**, *263*, 499.
(68) Midden-dorf, T. R.; Mazzola, L. T.; Lao, K.; Steffen, M. A.; Boxer, S. G. *Biochim. Biophys. Acta.* **1993**, *1143*, 223.
(69) Lathrop, E. J. P.; Friesner, R. A. *J. Phys. Chem.* **1994**, *98*, 3056.
(70) Atkins, P. W.; Trapp, C. A.; *Physical Chemistry*, 5th ed.; Oxford University Press: New York, 1994; pp C16.
(71) Scherer, P. O. J.; Fischer, S. F. *Chem. Phys.* **1989**, *131*, 115.
(72) Scherer, P. O. J.; Fischer, S. F.; Lancaster, C. R. D.; Fritzsch, G.; Schmidt, S.; Arlt, T.; Dressler, K.; Zinth, W. *Chem. Phys. Lett.* **1994**, *223*, 110.
(73) Artz, K.; Williams, J. C.; Allen, J. P.; Lendzian, F.; Rautter, J.; Lubitz, W. *Proc. Natl. Acad. Sci. U.S.A.* **1997**, *94*, 13582.
(74) Breton, J.; *The Photosynthetic Bacterial Reaction Center: Structure and Dynamics;* Breton, J., Verméglio, A. Eds.; NATO ASI Series, Series A: Life Sciences; Plenum: New York, 1988; p 59.
(75) Damjanović, A.; Ritz, T.; Schulten, K. *Phys. Rev. E* **1999**, *59*, 3293.